Ultrafast electron flux calibration for nanoscale dynamic imaging

Contact *w.a.bryan@swansea.ac.uk*

W. A. Bryan

Department of Physics, College of Science, Swansea University, Singleton Park, Swansea SA2 8PP.

A. R. Bainbridge

Accelerator Science and Technology Centre, STFC Daresbury Laboratory, Daresbury Science and Innovation Centre, Keckwick Lane, Daresbury, Cheshire WA4 4AD

Introduction

The far shorter wavelength of electrons as compared to photons of the same energy has long been recognized as revolutionary to imaging applications. Here we consider a low-energy form of electron microscopy whereby pulses of electrons are generated by an ultrafast (femtosecond) laser pulse [1,2]. Unlike photons, pulses of electrons are heavily dispersed in vacuum when there is on average more than one particle per pulse through the action of space-charge (SC). As a consequence, when trying to minimize the temporal resolution at the target under investigation, it is vitally important that the number of electrons per pulse is well known. The effect of SC is negated when there is on average less than one electron per pulse hence any electron flux calibration needs to be calibrated and sensitive down to the single particle level [3]. Here we demonstrate just such an observation requiring no assumptions about the experimental apparatus allowing the number of particles per electron pulse to be determined.

Experimental

A schematic of the emission process is given in figure 1, whereby a tungsten nanoscale metal tip (W-NSMT) is illuminated with low energy femtosecond laser pulses. The W-NSMT is formed from 0.25 mm diameter polycrystalline wire electrochemically etched to a point typically of tens of nanometers in diameter. Such NSMT are difficult to fabricate repeatably, a result of small variations of etchant concentration, temperature and etching activity caused by current and voltage fluctuations, along with an initially unknown crystal grain boundary alignment. As a consequence it is essentially meaningless to produce a NSMT, image with a TEM then transfer to our experimental chamber as the action of imaging will change the shape of the tip. Furthermore, tungsten oxide forms very rapidly, effectively blunting the NSMT.

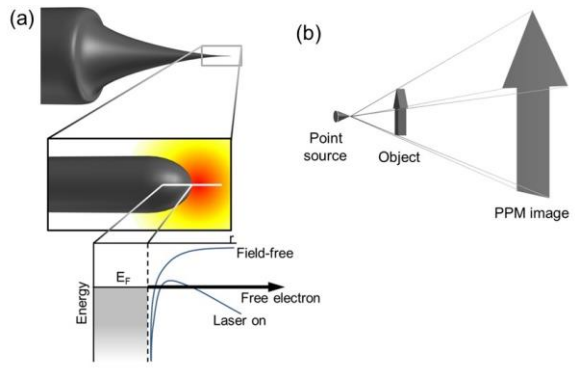

Figure 1. (a) Strong-field ionization from a nanoscale metal tip (NSMT) resulting in femtosecond pulses of electrons. The field enhancement at the apex of the NSMT confines emission to a region of tens of nanometers in diameter. Much as in atomic ionization by strong-field laser pulses, the distortion of the Coulomb barrier allows electrons at the Fermi level to tunnel directly into the continuum. (b) Schematic of Point-Projection Microscopy, which requires no lenses to magnify an object placed close to a point source, here the laser-illuminated NSMT.

It is the nanoscale radius of curvature which makes NSMTs so attractive a source for ultrafast electron pulses. Applying a femtosecond laser pulse (here from UFL1, EPSRC Laser Loan Pool as operated by the Lasers for Science Facility, STFC Rutherford Appleton Laboratory) initiates a field enhancement effect. Tuning the Light Conversion Orpheus-N non-collinear optical parametric amplifier to 800 nm and transmission focusing a 10% split of the resulting 20 fs to a spot of around 6 microns generates a peak intensity of between 10^{10} and 10^{12} Wcm^{-2}. The photon energy of 1.56 eV would require 3-photon emission to generate electrons directly from a planar surface, which at this intensity is highly unlikely. However, the nanometric radius of curvature causes at least a factor of ten enhancement to the electric field which pushes the effective intensity into the tunneling regime. Here, the laser field governs the time-dependent modification of the Coulomb barrier electrons at the Fermi level are influenced by, and at a sufficiently high intensity, a significant probability of tunneling through the now-finite barrier exists. The laser pulse is therefore a nonlinear electron switch.

Careful manipulation of the overlap of the laser focus and the very apex of the NSMT facilitates a control of the resulting electron flux. The NSMT is not placed at the peak of the field, rather we estimate it experiences an intensity a factor of 20 less than the peak. Initial experiments indicate that electron fluxes of up to 10^4 e/pulse can be maintained by a W-NSMT illuminated at a laser repetition rate of 1 kHz and ~10^2 at a repetition rate of 50 kHz, a consequence of the extreme hardness of the material. Such a calibration is possible by applying the necessary negative bias voltage to the NSMT via a femtoammeter (Keithley 6517B) or a charge-sensitive amplifier (Ortec 142B), allowing the departing charge to be determined. Following the discussion in the introduction, such e-pulses are not well suited to ultrafast electron microscopy or diffraction as SC will dominate. The femtoammeter is sensitive to currents in the fA range, however the NSMT is a highly efficient antenna, hence the RMS noise on the meter is of the order 100 fA at very best. As a result, the lowest averaged electron flux detectable with the femtoammeter corresponds to around 10 e/pulse at 50 kHz, and the charge-sensitive amplifier is noise-limited to of the order 100 e/pulse at 50 kHz.

Clearly, neither method will allow the identification of conditions suitable for generating single electron pulses (1e/pulse), hence we turn to an adaption of our imaging technique. For low-energy femtosecond point projection microscopy (fs-PPM) as used here, the ratio of the distances between source-target, and source-detector define the magnification as illustrated in figure 1(b). To achieve a magnification of greater than 1000 times, a source-target distance of less than a millimetre is required, thus defining the maximum voltage difference by vacuum breakdown to be below 1 kV, and typically around 300 V. Electrons of hundreds of electronvolts are significantly deflected by Earth's field hence the vacuum chamber is surrounded by three pairs of Helmholtz coils. Following interaction with the object to be

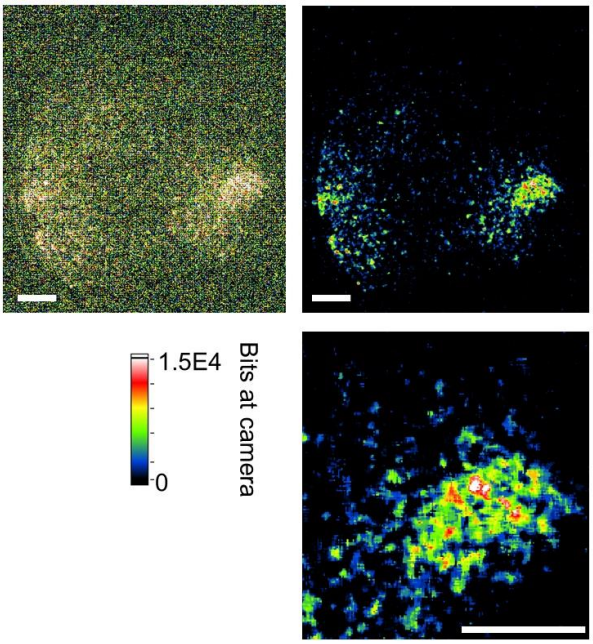

Figure 2. (a) Raw gauge electron image. (b) Median filtered gauge electron image. (c) magnification of (b) showing individual electron arrival points. The scale bar is 10 mm at the detector plane in all cases.

imaged, our electron pulses propagate through around 0.4 m of field-free vacuum to a pair of imaging-quality microchannel plates (MCPs, Burle) and a phosphor screen (PS, Kimball Physics). Electron pulses arriving at the MCP+PS detector apparatus are multiplied by between $10^{4.5}$ and 10^{6} depending on the voltage across the MCPs, typically between 1.0 to 1.5 kV. The resulting electron bunch is then converted to 450 nm photons on incidence on the PS following further acceleration to 5 keV, and imaged on an AVT Pike FireWire camera.

If the MCP+PS+window+lens+camera quantum efficiency were well known, direct calibration would in principle be possible. This is hampered however by both the MCP and PS performance degrading over time, hence such a recalibration would need to be performed regularly. Furthermore, a known emitter is necessary, and the effort required to mount, transport and characterize such a source is prohibitive.

We turn therefore to the UHV and imaging capabilities of our electron detector. The typical operating pressure of this instrument is 6×10^{-9} mbar, hence the detector is intrinsically low noise, typically registering less than one background count per second with the electron source off. Note this is over the full active area of the MCPs. Under typical operating conditions, the front of the MCP pair is negatively biased to between 10 and 20 V prevent stray electrons from our full-range pressure gauge (Pfeiffer HPT 100) being collected by our detector while still allowing fs-PPM electrons to pass. As variation of MCP efficiency with electron energy is known (80% at 300 eV to 50% at tens of eV), a count rate conversion can be applied between gauge electrons and laser-generated ultrafast electrons.

Before recording fs-PPM images we perform a simple calibration measurement: with NSMT not emitting but the MCP+PS set to operational conditions, we vary the voltage on the front of the MCP until the detector is collecting tens of *gauge* electrons per exposure (286 ms). Then, by manually counting the number of electrons per exposure, we have a route to converting signal at the AVT Pike to electrons arriving at the front of the MCP. This is illustrated in two stages, first the raw image as read directly from the Pike camera, fig 2(a), and secondly after a median filter had been applied to suppress single pixel noise, fig. 2(b). The individual electron arrivals can be seen in fig. 2(c).

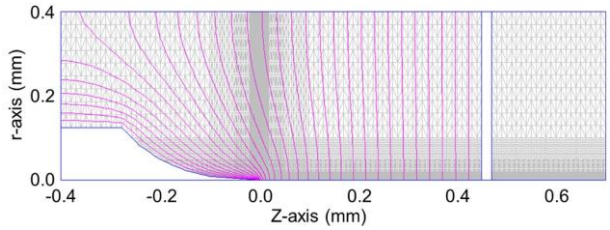

Figure 3. Example electrostatic field map of our NSMT (from left, apex at 0,0) and TEM grid (at 0.45 mm). The NSMT is held at -300 V with the TEM grid at 0 V. Electric field contours are separated by 10 V (magenta) and the underlying grid is shown in grey. High density grid points around the NSMT apex are seen.

Calibrated imaging comparison to numerical simulations

To fully understand the trajectory of electrons propagating through our instrument, we have carried out numeric simulations. An electrostatic model of the NSMT, target and field free flight region to the detector are modelled using Poisson Superfish (Los Alamos Accelerator Code Group), which is then imported into the General Particle Tracer (GPT, Pulsar Physics), used to model charged particle dynamics in EM fields. An example field map is given in figure 3, which illustrates the requirement for very tightly packed mesh points around the NSMT as compared to the macroscopic elements which are three orders of magnitude larger.

The time evolution of a propagating electron pulse is illustrated in figure 4, where each panel of the figure has been centred on the electron pulse as it propagates. The spatial spreading or stretching of the electron pulse is the result of the electrostatic field generated by the NSMT.

The GPT model is used to predict the distribution of electrons at the detector which is 0.441 m from the NSMT. We select a TEM grid (300 mesh Cu, bar spacing 85 μm, bar width 15 μm)

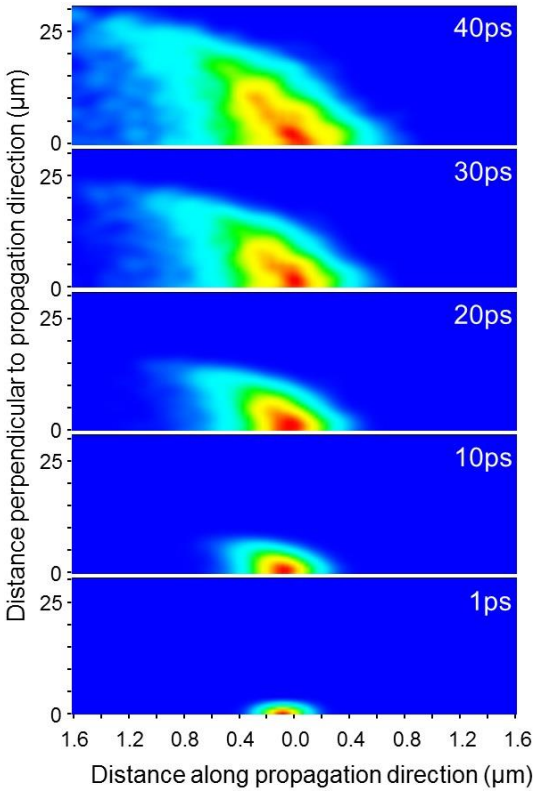

Figure 4. Femtosecond electron pulse propagation modelled with GPT (Pulsar Physics). The electron pulse is emitted at t = 0, and propagates from the NSMT along the field map shown in figure 3. At each frame presented, the distance along the propagation direction is zero'd to the centre of the pulse in time.

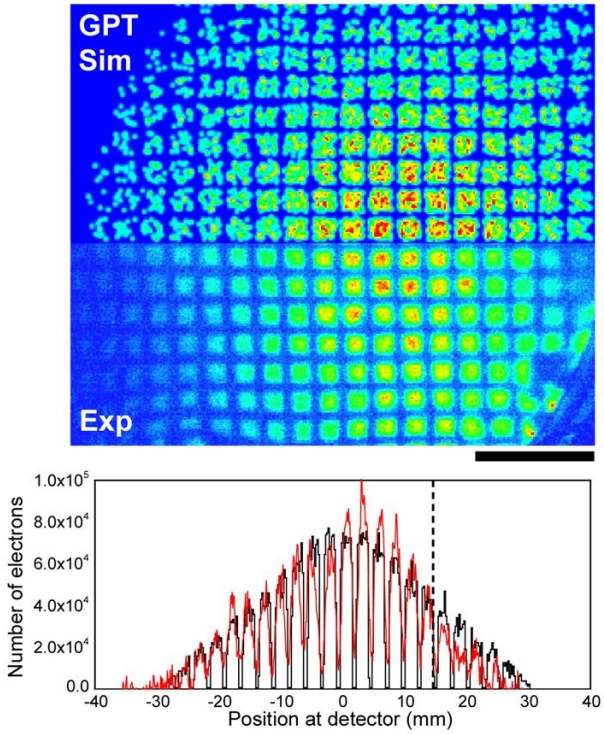

Figure 5. (top) GPT simulation of the propagation of a femtosecond electron pulse through a 300 mesh TEM grid placed 5 mm from the NSMT. (middle) Experimental observation of the same configuration. Scale bar is 15 mm at the detector plane. (bottom) Direct comparison between GPT model (black) and experimental measurements (red).

as the target as it allows easy calibration of magnification. The modelled distribution of electrons at the detector is shown in figure 5 (top). The only free parameter is the radius of the emission site at the end of the NSMT, which is here set to 11 nm. As the size of this site is varied, the predicted distribution width changes, and comparisons are made to experimentally measured distribution under the same conditions to define the site radius. The experimental distribution results from femtosecond electron pulses generated using UFL1, the distribution of electrons recorded at the MCP+PS+camera. The calibration discussed earlier is applied to find number of electrons in the image, shown in figure 5 (middle). As is apparent, the distribution of electrons is very similar, indicating our modelling describes the experiment well. To highlight this agreement, we take a section through the experimental and numerical results and directly overlap, as shown in figure 5 (bottom).

Conclusions

We have demonstrated an electron flux calibration method, here applied to femtosecond pulses of electrons. Such pulses are being employed for femtosecond electron microscopy, and to understand space-charge distortions in time and space, it is vital we are able to quantify down to single electrons per pulse, which has been shown here. We have also presented the degree to which the electron trajectories through our instrument agree with numerical modelling.

Acknowledgements

We are grateful to the staff and panel of the EPSRC Laser Loan Pool for their support of this work, specifically Ian Clark.

References

1. Gulde et al, *Science* **348** 200-204 (2014)
2. Muller et al, *Nature Communications* **5** 5292 (2014)
3. Lahme et al, *Structural Dynamics* **1** 034303 (2014)